Electrochimica Acta 290 (2018) 676–685

Contents lists available at ScienceDirect

Electrochimica Acta

journal homepage: www.elsevier.com/locate/electacta

Current and potential distribution in electrochemical reactors with activated or resistive electrodes. A multiregion and open source approach

A.N. Colli*, J.M. Bisang

Universidad Nacional del Litoral, CONICET, Programa de Electroquímica Aplicada e Ingeniería Electroquímica (PRELINE), Facultad de Ingeniería Química, Santiago del Estero 2829, S3000AOM, Santa Fe, Argentina

ARTICLE INFO

Article history:
Received 15 May 2018
Received in revised form
5 September 2018
Accepted 18 September 2018
Available online 19 September 2018

Keywords:
Resistive electrodes
Potential distribution
Bipolar electrodes
Current distribution
Leakage currents

ABSTRACT

An open source compact and general tool, implemented in OpenFOAM including a novel solver with a new boundary condition and post-processing utilities, is derived to enable calculations of local current and potential distributions in electrochemical systems with activated or resistive electrodes and also leakage currents in the case of a bipolar connection. The algorithm allows the calculations for a given local potential in any electrode, for a fixed cell potential difference and also for a current flowing through the cell under galvanostatic control. In order to validate the algorithm, a detailed comparison between the suggested strategy with experimental results and some simplified theoretical models is made. It was concluded that the proposed mathematical treatment is reliable for the modelling of these electrochemical systems due to the good agreement between theoretical and experimental values with a mean relative percent error of 8.8 ± 2.1% for the current distribution for the whole set of experiments.

1. Introduction

The current distribution in electrochemical reactors is largely determined by geometric factors [1], such as the shape of the cell, conductivities of solid and fluid phases and the placement of electrodes, called primary current distribution [2]. Additionally, it is affected by electrode kinetics, which depends on the electrocatalytic properties of the materials and on hydrodynamic conditions [3–6], defining the secondary and tertiary distributions. Electrochemical reactions proceeding at i) low conductivity electrodes, for example composite materials used in redox flow batteries [7,8], or ii) activated thin metal foils or sheets, of finite resistivity [9] able to work at high current densities [10], can generate marked current and potential distributions. Under these conditions, the production capacity per unit electrode area decreases, the product selectivity is affected and also wasting power takes place. Therefore, in the design of an electrochemical reactor, the electrical resistance of the electrodes and their geometric dimensions must be carefully chosen to minimise costs. Two other areas where the current distribution is crucial are the electroplating of small objects and electrochemical machining. In the first case the thickness of the coatings is non-uniform altering the quality of the product and in the second one the accuracy of the process is affected. Regarding redox flow batteries, previously has been demonstrated that considerable gains in performance have been achieved by reducing the ohmic resistances of the cell, via increasing the compression of the felt electrode and decreasing the contact resistance within the cell [11,12]. Thus, a study of the influence of different ways of feeding resistive terminal electrodes is desirable.

Theoretical analysis of current-potential distribution in electrochemical reactors has been one of the major subjects in electrochemical engineering. The effect of electrode resistance on the current-potential distribution has been discussed in the past for geometries such as wires [13], cylindrical forms [14,15] or rectangular ducts [16], where a 1D variation of potential drop into the electrodes is only necessary. Moreover, most of the so far reported efforts focusing on modelling current-potential distributions for electrochemical cells by computational fluid dynamics (CFD) assume the practical condition that the specific conductivity of the solid phase is much higher than those of the fluid phase. Calculations were made in the framework of the finite element method (FEM) using the commercial software Comsol Multiphysics [17,18],

* Corresponding author.
E-mail address: ancolli@gmail.com (A.N. Colli).

https://doi.org/10.1016/j.electacta.2018.09.121
0013-4686/

with the finite difference approach (FDM) [19], finite volume method (FVM) using open source code [20] or authors' routines [21].

Since boundary conditions at the electrode surface of monopolar or bipolar electrodes with finite specific conductivity cannot be formulated explicitly (the potential of the solid phase is not uniform and unknown *a priori*), the current density on them must be obtained from iterative calculations. A problem like this is too complex to be routinely resolved by a closed-form solution. Apart from the simple geometries and simple kinetic and mass-transfer conditions, problems of current distribution can be solved only through numerical techniques [22]. For over 30 years, numerical simulations have become central to a vast range of scientific areas. As an important tool for predictive process design and for the scale-up of cells and processes (and scale-down of industrial processes for laboratory testing), simulations and modelling can replace a large number of experiments. Additionally, simulations allow sensitivity analysis of different parameters to direct research efforts to obtain most significant improvements.

The goal of this paper is to provide a general strategy (solver-boundary condition) based on solving the potential field for the solid (electrodes) and fluid (solution) phases, coupling both by the electrochemical kinetics in order to design and/or evaluate electrochemical systems composed of monopolar or bipolar electrodes with finite specific conductivity with the help of the freely available CFD-toolbox OpenFOAM [23]. It is also the aim to compare the results obtained by the proposed tool with some of the limiting predictions that have been made in previous theoretical treatments of simplified problems and with previous experimental results for the monopolar case and own results for the bipolar case.

2. Theoretical considerations

2.1. Multiregion approach

A multiregion approach involves coupled physics of dissimilar continua (e.g. fluid-solid). In the multiregion method, separate governing equations for the multiphysics in each region are solved. Fig. 1 shows two blocks for the electrochemical computational calculations, where separate governing potential equations will be solved for Region 1, solid phase, and Region 2, fluid phase. Both regions are related by a common boundary patch or interface where the potentials on each phase are coupled by the electrochemical kinetics. In the present contribution these calculations were performed developing a novel solver with a new boundary condition based on the finite volume method (FVM) with the help of the OpenFOAM's multiregion functionality.

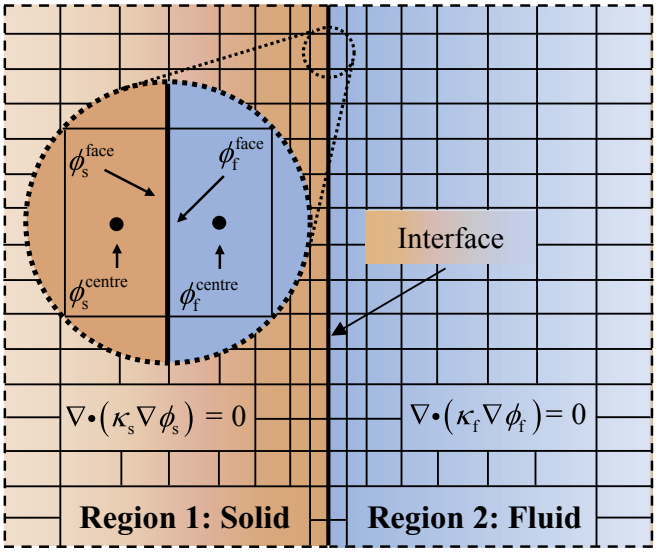

Fig. 1. Graphical representation of a multiregion approach, showing the discretisation near the solid (s) - fluid (f) interface for a non-uniform structured grid.

A general electrochemical system composed of electrodes, electrolyte, separators and the container with insulating walls is considered. As main difference with previous publications [19–21], is that the restriction about specific conductivity of the electrodes must be much higher than that of the electrolyte, equipotential solid phase assumption, is no longer needed. For each phase, the divergence of the current density is null and neglecting the concentration gradients the Laplace equation is valid [1]

$$\nabla\cdot\left(\kappa_{f\text{-}s}\nabla\phi_{f\text{-}s}\right) = 0 \tag{1}$$

where ϕ represents the local electrical potential in the fluid (f) or solid (s) region and κ its electrical conductivity. The presence of a separator or the existence of bubbles as a consequence of gas evolution reactions can be taken into account by means of an effective conductivity in Eq. (1) for the fluid phase. However, novel designs of electrochemical reactors propose to divert the gas phase mainly to the backside of the electrode [24,25] avoiding its accumulation in the interelectrode gap along the electrode length. Likewise, the increase in both the working pressure, in order to diminish the size of the gas bubbles [26], and the electrolyte flow rate also restricts the influence of the gases evolved at the electrodes on the reactor behaviour. Consequently, the gas-phase will be disregarded in the present mathematical model. Analogously, the use of thin layers of different catalysts in the solid phase can be specified in Eq. (1) through its thickness and conductivity. ϕ is a scalar function of space whose gradient, a vector called electric field is associated with flow of current. Consequently, Laplace's equation expresses the condition of conservation of current in a region free of other charges.

The current density in the fluid phase is determined by the ionic flux, which is described in terms of diffusion across a concentration gradient and migration down the electric field [27]. The absence of concentration gradients in the present proposal relates these calculations with the secondary current distribution approach presented in previous experimental and theoretical treatments.

Equation (1) will be solved by the finite volume method [28,29] for each region, with proper boundary conditions, BC, starting from initial guess values and solving sequentially for each region until convergence is reached.

2.2. Boundary conditions

Both solid and fluid regions, sketched in Fig. 1, have several patches for which boundary conditions have to be specified. Therefore, at the solid-fluid interface take place electrochemical reactions setting a discontinuity in the potential field. There is a relationship, usually non-linear, between the potential drop across this interface and the crossing current. According to Faraday's law of electrolysis, the flow of current through a fluid-solid interface gives the rate of the electrochemical reaction, which must be equated to the current density according to application of Ohm's law in both phases. In this way, the current density, j, at any point of the electrode is determined by the local potential gradient at each boundary patch, bp, the electrical conductivity of each region and the flux of all species, which can be expressed by the following equation

$$\kappa_s \frac{\partial \phi_s}{\partial n}\bigg|_{bp_s} = -\kappa_f \frac{\partial \phi_f}{\partial n}\bigg|_{bp_f} = j_k \tag{2}$$

Eq. (2) corresponds to a coupling boundary condition. Here, n represents the coordinate normal to the boundary in direction of the interior of each phase and j_k is given by

$$j_k = \sum_i j_k^i \tag{3}$$

being

$$j_k^i = g\left(T, j_0^i, b^i, \phi_{s,k}, \phi_{f,k}, E_0^i\right) \tag{4}$$

where T is the temperature, j_0^i is the exchange current density, b^i is the Tafel slope and E_0^i is the equilibrium potential for each ith electrochemical reaction. In the above non-linear relationship the subscript k denotes the anodic or cathodic interface and the superscript characterises the ith electrochemical reaction at it. Thus, $\phi_{s,k}$ and $\phi_{f,k}$ are the solid-side and fluid-side potentials at the kth interface, respectively.

At insulating walls or symmetry axes, w, the gradient of electrical potential normal to the boundary vanishes due to no flux of species, and then equation (2) is simplified to

$$\frac{\partial \phi_{f\text{-}s}}{\partial n}\bigg|_w = 0 \tag{5}$$

yielding a Neumann boundary condition. Finally, the set of boundary conditions is completed considering the region for current feeder, CF, at each terminal electrode, which depends on the type of electrical control. Thus, for a fixed cell potential difference and for a given local potential in any electrode point, pseudo-potentiostatic control, a Dirichlet boundary condition is valid according to

$$\phi_{f\text{-}s}\big|_{CF} = \text{constant} \tag{6}$$

where the constant is assumed zero at the cathodic current feeder and equal to the cell potential difference, U, at the anodic part. Under galvanostatic control, current feeders are fed at a fixed known current, I, and a Neumann boundary condition must be used for the anodic current feeder, in accordance with

$$\kappa_s \frac{\partial \phi_s}{\partial n}\bigg|_{CF} = \frac{I}{\text{feeder cross-section area}} \tag{7}$$

whereas a Dirichlet boundary condition, Eq. (6), is appropriate for the cathodic current feeder imposing 0 as its potential.

By discretising previous equations, (1) to (7), via the finite volume method and taking into account Fig. 1, the derivative on the left hand side of Eq. (2) can be linearised by the ratio between the potential difference in the patch, $\phi_{s-f,k}^{face} - \phi_{s-f,k}^{centre}$, divided by the distance between the cell centre to the interface, Δ. Additionally, applying a Taylor series expansion to the right hand side of Eq. (2) and neglecting high order terms yields

$$\pm\frac{\kappa_{s\text{-}f}}{\Delta}\left(\phi_{s\text{-}f,k}^{face} - \phi_{s\text{-}f,k}^{centre}\right) = \sum_i \left[j_k^i - \phi_{s\text{-}f,k}^{face}\frac{dj_k^i}{d\phi_{s\text{-}f,k}^{face}}\right]_{\phi_{s\text{-}f,k}^{face,0}} + \sum_i \frac{dj_k^i}{d\phi_{s\text{-}f,k}^{face}}\bigg|_{\phi_{s\text{-}f,k}^{face,0}} \phi_{s\text{-}f,k}^{face} \tag{8}$$

this corresponds to a Robin BC for each phase. Henceforth, the upper sign is valid for solid phase and the lower sign for fluid phase. $\phi_{s\text{-}f,k}^{center}$ represents the potential at the solid or fluid phase in the centre of the volume element located immediately near the interface and $\phi_{s\text{-}f,k}^{face,0}$ is the solid-side or fluid-side potential at the kth interface extracted from the available data at the previous iteration step, denoted with the superscript 0. Isolating $\phi_{s\text{-}f,k}^{face}$ from Eq. (8) is

$$\phi_{s\text{-}f,k}^{face} = \pm\frac{\sum_i B_k^i}{1 \mp \sum_i A_k^i} + \frac{1}{1 \mp \sum_i A_k^i}\phi_{s\text{-}f,k}^{centre} \tag{9}$$

where

$$\sum_i B_k^i = \frac{\Delta}{\kappa_{s\text{-}f}}\sum_i \left[j_k^i - \phi_{s-f}^{face}\frac{dj_k^i}{d\phi_{s\text{-}f,k}^{face}}\right]_{\phi_{s\text{-}f,k}^{face,0}} \tag{10}$$

and

$$\sum_i A_k^i = \frac{\Delta}{\kappa_{s\text{-}f}}\sum_i \frac{dj_k^i}{d\phi_{s\text{-}f,k}^{face}}\bigg|_{\phi_{s\text{-}f,k}^{face,0}} \tag{11}$$

2.3. Boundary conditions implemented in OpenFOAM

A Robin BC can be seen as a weighted combination of Dirichlet BC and Neumann BC. OpenFOAM has pre-defined Dirichlet BC called fixedValue for Eq. (6) and Neumann BCs called zeroGradient, for Eq. (5) or fixedGradient, for Eq. (7), respectively. There is a boundary condition called mixed, which is mainly used for switching between the fixed value and the fixed gradient situations on a particular boundary and it is given by the following expression

$$\phi_{s\text{-}f,k}^{face} = f\ VR + (1-f)\left(\phi_{s\text{-}f,k}^{centre} + VGR\ \Delta\right) \tag{12}$$

f is the fraction Expression defined by the user. When $f = 1$, Eq. (12) gives a Dirichlet boundary condition and for $f = 0$ it yields a Neumann one. The Robin case is represented by $0 < f < 1$, being f calculated as explained below. By comparing Eq. (9) with Eq. (12) it is obtained for each interface

$$VGR_{s\text{-}f} = 0 \tag{13}$$

$$f_{s\text{-}f} = \pm\frac{\sum_i A_k^i}{1 \pm \sum_i A_k^i} \tag{14}$$

$$VR_{s\text{-}f} = \frac{-\sum_i B_k^i}{\sum_i A_k^i} \tag{15}$$

For the present simulations and further comparisons with experimental results, just irreversible gas evolving reactions are considered at each interface, thus the current density can be expressed as a Tafel equation according to

$$j_k = \sum_i j_0^i \exp\left(\frac{\phi_{s,k}^{face} - \phi_{f,k}^{face} - E_0^i}{b^i}\right) \tag{16}$$

In the following, both kinetic parameters will be considered positive for anodic reactions and negative for the cathodic case in order to retain the usual sign convention for current density.

Table 1
Physicochemical properties and kinetic parameters used in the modelling.

Property	Value	Measured/Calculated
κ_f [NaOH] = 0.1 M (S m^{-1})	2.27	Experimentally [14]
κ_f [NaOH] = 1 M (S m^{-1})	18.5	Experimentally
κ_f [NaOH] = 6 M (S m^{-1})	41.2	Experimentally
κ_s [resistive electrode] (S m^{-1})	287	Calculated
κ_s [Pt] (S m^{-1})	9.1×10^6	Literature
κ_s [Ni] (S m^{-1})	1.45×10^7	Literature
U_0 (V)	1.23	Theoretically [21]
b_a (V)	4.85×10^{-2}	Experimentally [20]
$j_{0,a}$ (A m^{-2})	9.38×10^{-2}	Experimentally [20]
b_c (V)	-6.08×10^{-2}	Experimentally [20]
$j_{0,c}$ (A m^{-2})	-6.95×10^{-1}	Experimentally [20]

Combining Eq. (11) with the derivative of Eq. (16) gives

$$\sum_i A_k^i = \pm\frac{\Delta}{\kappa_{s\text{-}f}} \sum_i \frac{j_0^i}{b^i} \exp\left(\frac{\phi_{s,k}^{face} - \phi_{f,k}^{face} - E_0^i}{b^i}\right) \tag{17}$$

Combining Eqs. (14) and (17) gives

$$f_{s\text{-}f} = \frac{\sum_i \frac{j_0^i}{b^i} \exp\left(\frac{\phi_{s,k}^{face} - \phi_{f,k}^{face} - E_0^i}{b^i}\right)}{\frac{\kappa_{s\text{-}f}}{\Delta} + \sum_i \frac{j_0^i}{b^i} \exp\left(\frac{\phi_{s,k}^{face} - \phi_{f,k}^{face} - E_0^i}{b^i}\right)} \tag{18}$$

Introducing Eqs. (10) and (11) into Eq. (15) and taking into account Eqs. (16) and (17) results in

$$VR_{s\text{-}f} = \phi_{s-f,k}^{face,0} \mp \frac{\sum_i j_0^i \exp\left(\frac{\phi_{s,k}^{face} - \phi_{f,k}^{face} - E_0^i}{b^i}\right)}{\sum_i \frac{j_0^i}{b^i} \exp\left(\frac{\phi_{s,k}^{face} - \phi_{f,k}^{face} - E_0^i}{b^i}\right)} \tag{19}$$

Then, the set of general equations (12)–(15), valid for any number of reactions and kinetic controls, is replaced by the set of Eqs. (12), (13), (18) and (19) for our particular case.

For the above calculation procedure is not necessary to propose a current distribution at each interface as guess value [21], or to impose as constraint current conservation in bipolar electrodes [20,30]. Therefore, the number of iterations and the computation time is diminished, showing always convergence, which can be recognised as an important advantage of this numerical calculation

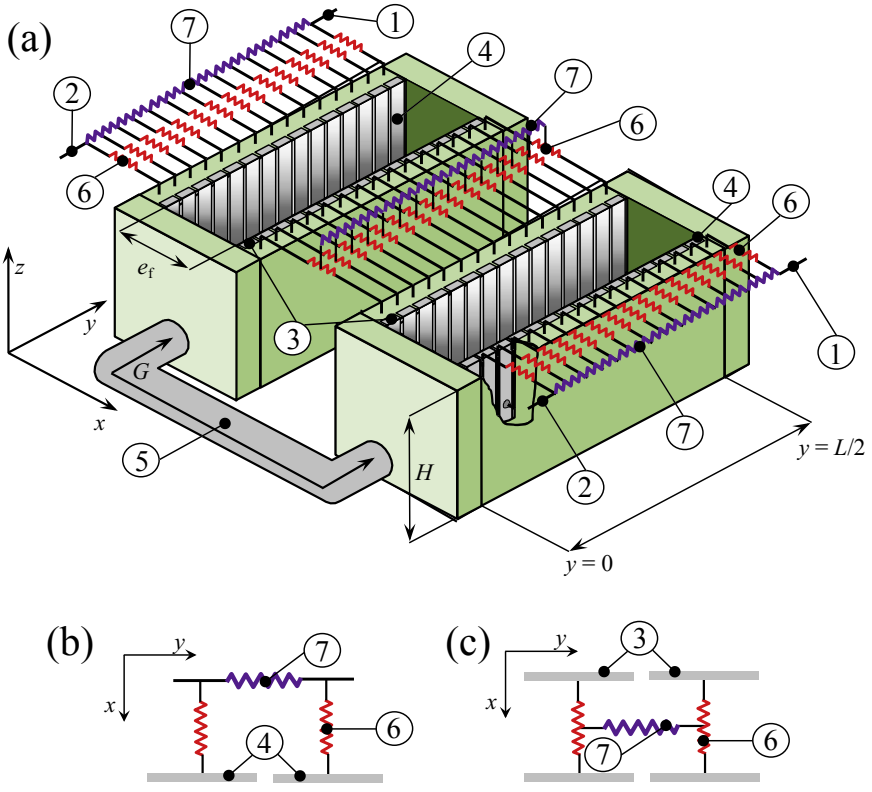

Fig. 2. Part (a): Schematic representation of an electrochemical stack composed of terminal and a bipolar resistive electrodes. (1) Current feed from the middle part of terminal electrodes; (2) current feed from the extremes of terminal electrodes; (3) bipolar electrode; (4) terminal electrode; (5) electrolyte manifold; (6) calibrated resistors made of constantan wires (in red); (7) commercial metal film resistors (in purple). Part (b): electrical arrangement to simulate the terminal electrodes. Part (c): electrical arrangement to simulate the bipolar electrode.

procedure. Additionally, this methodology also presents a high simplicity when a large number of electrodes are considered. Several strategies of electrical control were used such as: current imposed to the reactor (galvanostatic control), fixed cell potential difference or the adoption of a given local potential in any electrode. In all cases the current distribution at each electrode is reported together with the cell potential difference, total current and leakage current depending on the electrical control approach. The current drained by the kth electrode with a surface area of S_k is given by

$$I_k = \int_{S_k} j_k dS_k \tag{20}$$

The physicochemical properties and kinetic parameters used in the modelling are summarised in Table 1.

The present strategy is supplied as GitHub link [31] in order that the reader makes use of it. Thus, a novel solver, a new BC and a post-processing utility, that allow calculating current distribution at each electrode and leakage currents, is brought. Input parameters are geometry, conductivity of each phase and kinetic parameters for each ith electrochemical reaction per electrode. Finally, a concise example and a tutorial on how to use the validated tool are provided, which have been tested in OpenFOAM 5.0, OpenFOAM 6 and OpenFOAM-dev [32].

3. Materials and methods

The experimental setup was composed of two undivided reactors electrically connected in series, as shown schematically in Fig. 2, which constitutes a bipolar electrochemical stack with one bipolar electrode. Usually, this type of cell has symmetrical inlet and outlet manifolds, and thus only one half of the stack was considered. The inlet manifold was simulated by a Teflon tube, which interconnects the electrolyte in the reactors. With the aim of searching for the effect of the by-pass resistance two types of Teflon tubes, whose geometrical dimensions are given in Table 2, and two different electrolyte concentrations were used. Hence four by-pass resistances were examined. The current density distribution was determined using the segmented electrode method, and hydrogen- and oxygen-evolution from approximately 1 M NaOH or 6 M NaOH were the cathodic and anodic reactions. The electrodes at each reactor were formed with 15 nickel segments, 6.1 mm wide and 50 mm high, H, which were insulated from one another by an epoxy resin of about 0.5 mm thick. Short electrodes were used in order to have a small amount of gases at the top minimising its influence on the current distribution. The interelectrode gap, e_f, was 20 mm and the segments were trimmed to make a reactor of 100 mm in length, $L/2$. The electrical arrangement to simulate the resistive electrodes is depicted on the bottom in Parts (b) and (c) of Fig. 2. Thus, commercial 1% metal film resistors of 0.22 Ω resistance, shown in purple, were intercalated between segments in y-axis direction, whereas calibrated resistors, 0.0255 Ω resistance, were connected to the backside of each segment, shown in red, in x-axis direction. This electrical arrangement simulates a resistive electrode of approximately 2 mm thickness with 287 S m^{-1} resistivity, typical values for a redox flow battery [33,34]. The current distribution at each electrode was determined by measuring the ohmic drop in the calibrated resistors, which were made from a constantan wire, 10 mm long, 1.5 mm diameter. The data acquisition was performed using a computer-controlled, home-made analogue multiplexer and five independent data sets were obtained for each controlled current. A dc power supply was used to apply a constant current to the feeders. The temperature in all experiments was approximately 27 °C. The electrical connection at each terminal electrode was made in only one point and two different positions were examined, as schematised in Fig. 2. Connection point 1 corresponds to the current feeder in the middle point of the electrode and connection 2 when it is placed at one end near the by-pass channel.

Table 2
Geometrical parameters of the by-passes.

Type	$A_m \times 10^{-4}$ (m^2)	G (m)
I	0.739	0.189
II	2.986	0.196

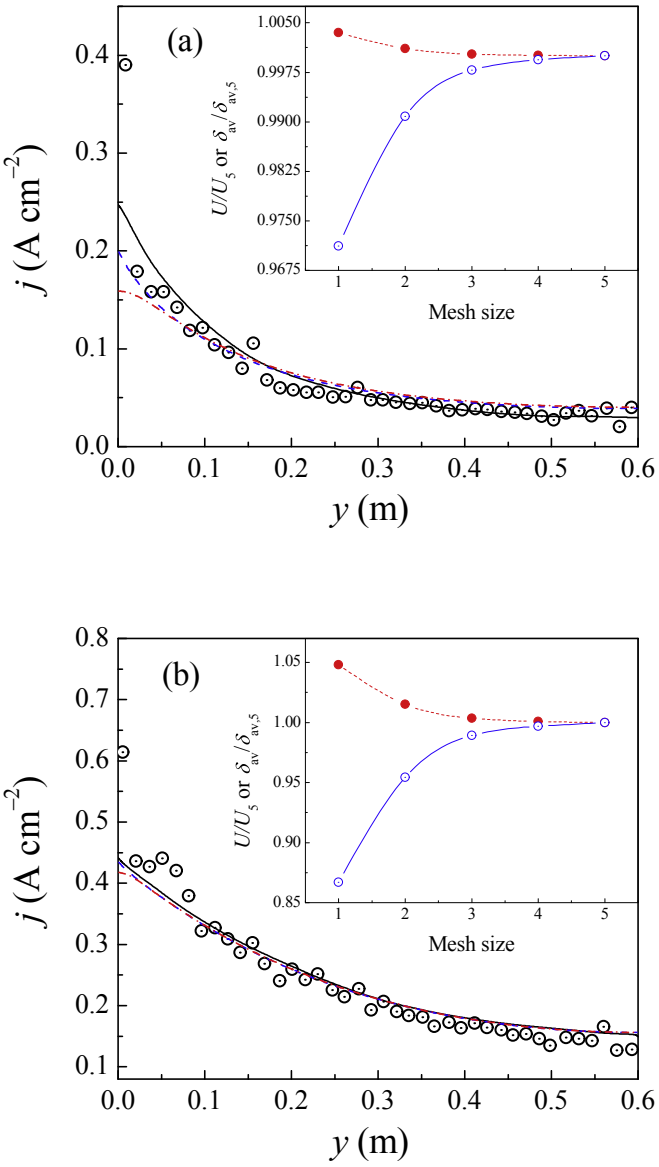

Fig. 3. Experimental and theoretical current distribution for a cylindrical electrochemical reactor. Hydrogen evolution at the inner electrode and oxygen evolution at the outer electrode from alkaline electrolytes. $T = 30$ °C. Part (a): [NaOH] = 1 M and $I = 0.269$ A. Part (b): [NaOH] = 0.1 M and $I = 0.896$ A. Full lines: analytical treatment from Ref. [35]. Dashed lines: numerical calculation at the inner electrode. Dash-dotted lines: numerical calculation for the outer electrode. Symbols: experimental values. Insets: mesh-independence study as a function of the mesh size given in Table 3. Open blue circles: $\delta_{av}/\delta_{av,5}$ for the inner electrode. Full red circles: U/U_5. Part (a): $U_5 = 1.922$ V; inner electrode $\delta_{av,5} = 0.417$. Part (b): $U_5 = 2.989$ V; inner electrode $\delta_{av,5} = 0.282$. The subscript 5 denotes mesh size 5 according to Table 3.

4. Results and discussion

4.1. Model validation by comparison with previous theoretical and experimental results

Fig. 3 compares experimental current density distributions [14,15], obtained in a cylindrical electrochemical reactor using the segmented counter electrode method, with theoretical predictions. The full line corresponds to the results of an analytical treatment based on the simultaneous solution of the potential distribution equation for the solid phase of the inner electrode together with the Laplace equation for the fluid phase [35]. In this last contribution, the counter electrode was assumed as equipotential and the electrochemical reaction at it presents a low polarization resistance. The dashed lines show the current distribution at the inner electrode according to the present numerical procedure and the dash-dotted lines for the counter electrode multiplied by the ratio between the surface areas of the outer and inner electrodes.

It can be observed that the proposed calculation strategy can reproduce both the experimental and analytical results. However, the numerical distributions are less marked than that of the analytical treatment as a consequence of the polarization resistance was disregarded at the counter electrode in this last theoretical model. As expected, this effect is more marked as smaller is the

Table 3
Mesh properties and computational characteristics.

Mesh size	Equidistant number of points in the radial-axial directions (r,z)			$I = 0.269$ A [NaOH] = 1 M		$I = 0.896$ A [NaOH] = 0.1 M	
	Inner Solid	Fluid	Outer Solid	t (s)[a]	n° iter.[b]	t (s)[a]	n° iter.[b]
1	(3,75)	(50,75)	(10,75)	0.6	107	0.8	264
2	(5,150)	(100,150)	(20,150)	5	111	6	283
3	(10,250)	(200,250)	(40,250)	34	153	28	274
4	(15,300)	(300,300)	(60,300)	136	338	62	266
5	(20,400)	(400,400)	(80,400)	353	365	171	316

[a] Obtained on a 2.5 GHz single core.
[b] Starting with 0 V for the inner electrode, 3 V for the outer electrode and 1.5 V for the fluid region.

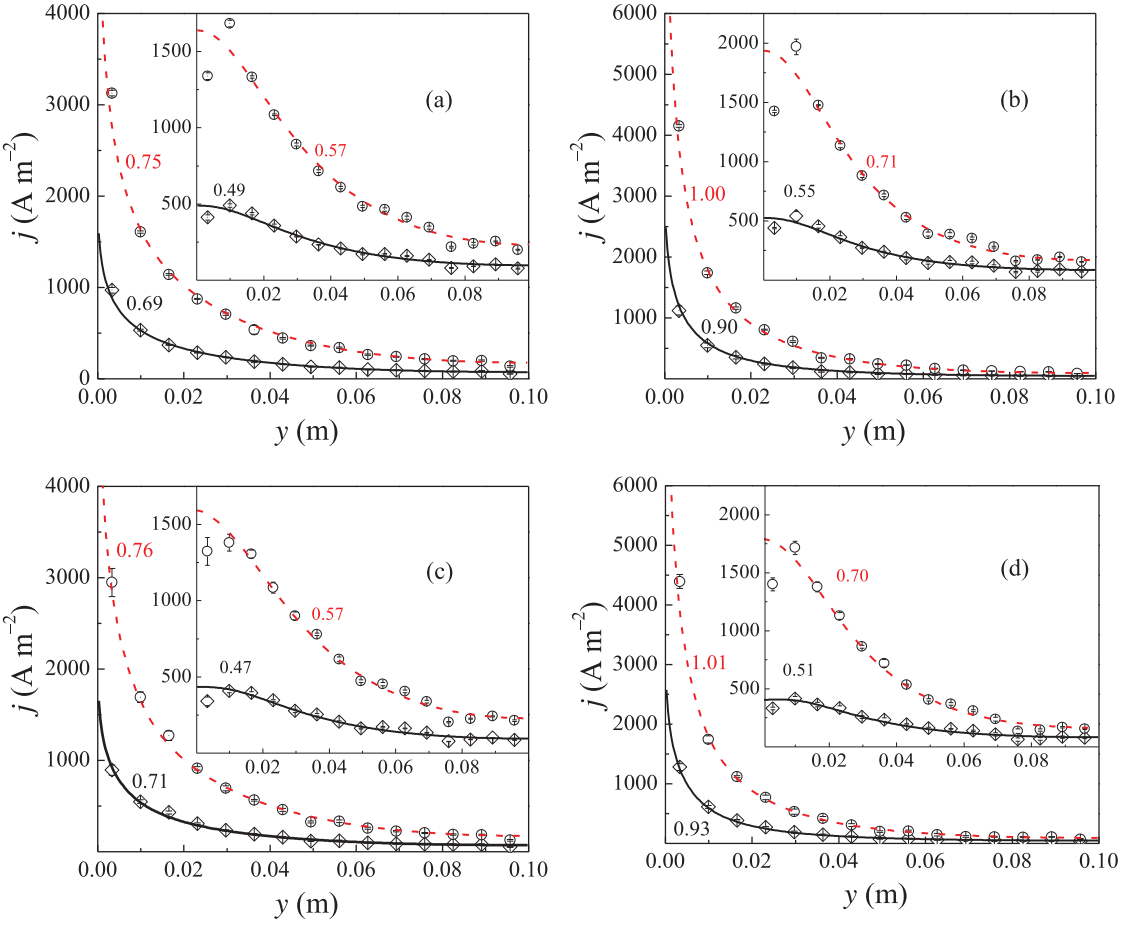

Fig. 4. Experimental and theoretical current distributions for a bipolar electrochemical stack with resistive electrodes. Water electrolysis from alkaline electrolytes. $T \approx 27$ °C. Current feeders placed at the end of the terminal electrodes. Part (a): By-pass I and [NaOH] = 1 M. Part (b): By-pass I and [NaOH] = 6 M. Part (c): By-pass II and [NaOH] = 1 M. Part (d): By-pass II and [NaOH] = 6 M. Symbols: experimental results. Error bars: confidence interval. Full black lines: numerical calculations at $I = 1$ A. Dashed red lines: numerical calculations at $I = 3$ A. Insets: current distributions for the bipolar electrode. Numbers at each curve: mean relative deviation.

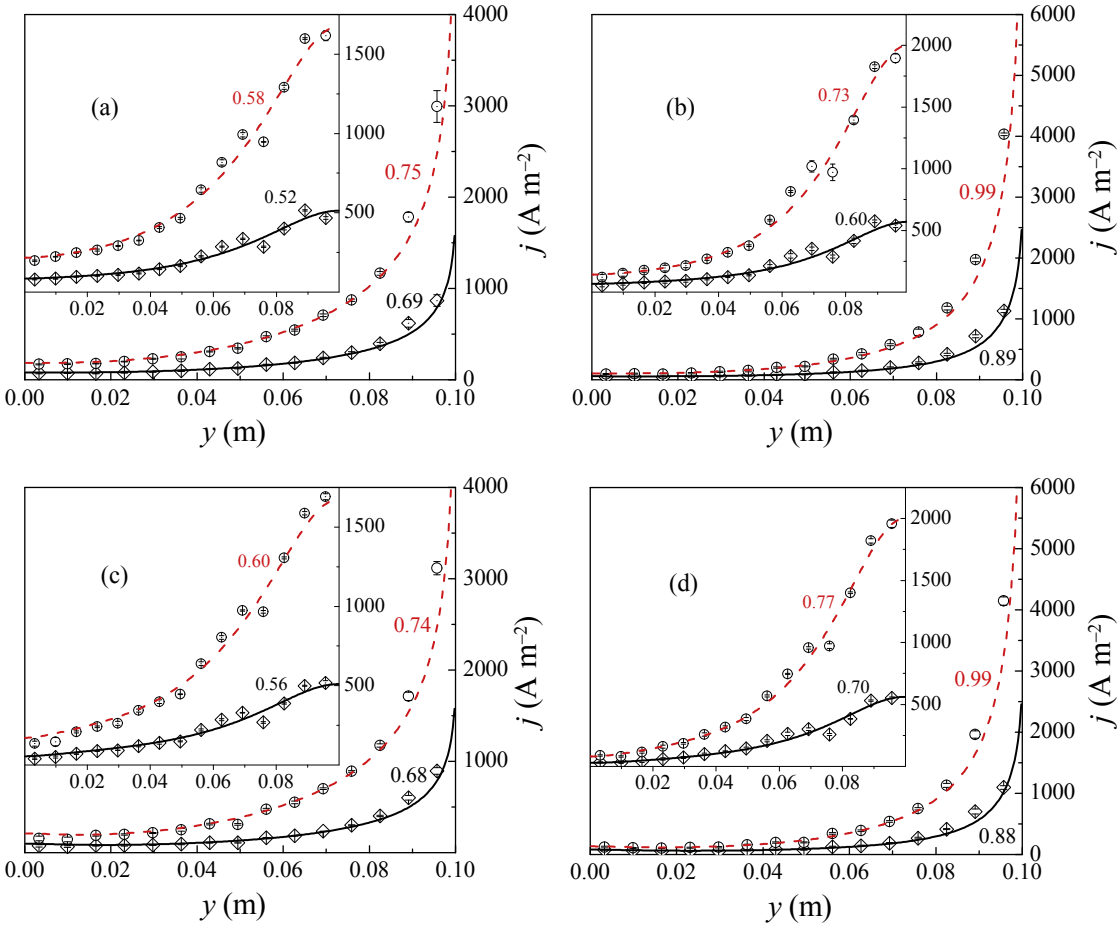

Fig. 5. Experimental and theoretical current distributions for a bipolar electrochemical stack with resistive electrodes. Water electrolysis from alkaline electrolytes. $T \approx 27\,^{\circ}C$. Current feeders placed in the middle point of the terminal electrodes. Part (a): By-pass I and [NaOH] = 1 M. Part (b): By-pass I and [NaOH] = 6 M. Part (c): By-pass II and [NaOH] = 1 M. Part (d): By-pass II and [NaOH] = 6 M. Symbols: experimental results. Error bars: confidence interval. Full black lines: numerical calculations at $I = 1$ A. Dashed red lines: numerical calculations at $I = 3$ A. Insets: current distributions for the bipolar electrode. Numbers at each curve: mean relative deviation.

total current. At a higher current, giving small polarization resistance values at the counter electrode, it is detected a very close agreement between numerical and analytical calculations. Thus, it can be stated that the rigorous numerical solution of the fundamental equations, above declared, validates the assumptions made by the analytical procedure. The numerical results in Fig. 3 also shows that the current distribution at the counter electrode is slightly more uniform than at the inner electrode, due to the fact that the solution phase resistance dampens the distribution. Likewise, the slope of the numerical calculated current distribution in the inner electrode at the reactor inlet is higher than that of the outer electrode. This finding can be explained taking into account that the current densities at the inner electrode are higher than the values at the outer one, giving a high polarization resistance in the latter. This high additional resistance at the outer electrode becomes more uniform the distribution in the inlet.

4.2. Mesh properties, computational characteristics and mesh-independence study

Table 3 displays the mesh sizes tested in the present calculations with the corresponding clock time and number of iterations needed, on a 2.5 GHz single core, to reach the final solution with a normalised tolerance of 1×10^{-7} for the potential field in each region. The initial guess values were 0 V for the inner solid region, 3 V for the outer solid region and 1.5 V for the fluid region and applying at the current feeder of the outer solid region the boundary condition given by Eq. (7).

To quantify the uniformity in the current distributions the mean relative deviation, δ_{av}, is defined as [6]

$$\delta_{av} = \frac{2}{L}\int_{0}^{L/2}\left|\frac{j}{j_{av}} - 1\right| dy \tag{21}$$

The insets in Fig. 3 a) and 3 b) show the results of a mesh-independence study, where the ratios of U and δ_{av} against the corresponding values for the finest mesh are plotted. It can be observed that in all cases the size of the mesh is adequate due to the imperceptible change of results when the mesh is refined.

4.3. Experimental and theoretical current distributions in a bipolar electrochemical stack with resistive electrodes

Fig. 4 displays typical current distributions for the reactor sketched in Fig. 2 with the current feeder in the border of each terminal electrode under different working conditions. Fig. 5 shows the same information with the current feeder in the middle point. Table 4 compares the theoretical with the experimental values for the potential cell difference and leakage current. In all cases reported in Figs. 4 and 5 it can be observed an excellent agreement between theoretical and experimental results. The same conclusion

Table 4
Summary of experimental results.

	[NaOH] (M)	Electrical connection	I (A)	U_{exp} (V)	CI_{exp} (V)	U_{the} (V)	I^*_{exp} (mA)	CI_{exp} (mA)	I^*_{the} (mA)	Ω^T_{av}(%)	Ω^{bip}_{av}(%)
By-pass I	1	Border	1	5.799	0.097	5.643	21.3	2.2	20.2	4.7	10.2
			3	9.606	0.037	9.430	32.4	0.6	31.2	5.8	8.4
		Middle point	1	5.838	0.065	5.656	18.6	1.2	15.0	8.2	9.9
			3	9.543	0.044	9.452	20.9	0.8	16.9	6.9	6.5
	6	Border	1	5.230	0.044	5.032	34.2	1.4	41.3	10.4	11.8
			3	7.865	0.030	7.490	43.2	0.5	56.5	7.7	10.8
		Middle point	1	5.194	0.029	5.049	29.4	2.3	32.7	11.5	11.8
			3	7.680	0.056	7.512	19.9	0.8	34.8	10.1	7.5
By-pass II	1	Border	1	5.774	0.029	5.588	73.4	1.4	77.0	5.9	10.0
			3	9.510	0.055	9.332	123.3	1.0	119.3	5.7	5.7
		Middle point	1	5.716	0.074	5.650	56.3	2.0	56.4	10.4	12.1
			3	9.308	0.080	9.450	68.3	0.6	64.1	9.7	9.5
	6	Border	1	5.194	0.046	4.960	147.6	2.1	156.7	8.2	10.5
			3	7.644	0.107	7.400	207.4	1.6	215.6	7.6	8.7
		Middle point	1	5.278	0.048	5.040	111.4	2.8	120.4	10.6	10.7
			3	7.720	0.067	7.510	118.1	0.9	130.3	9.5	7.2

can be obtained when the qualitatively information is quantified by means of the mean relative percent error between the theoretical and experimental current distributions, defined as

$$\Omega_{av} = \frac{100}{p}\sum_{1}^{p}\left|\frac{j^p_{exp}}{j^p_{the}} - 1\right| \quad (22)$$

where p is the pth segmented electrode. Ω_{av} is shown as last two columns in Table 4 for the terminal and bipolar electrodes, respectively, giving an average value of 8.8 ± 2.1% for the whole set of experiments.

The numbers at each curve in Figs. 4 and 5 represents δ_{av}, defined by Eq. (21), being the current distribution more uniform when this statistical parameter is smaller [6]. The current distributions for each terminal electrode are very similar; consequently only one curve is showed. As expected, the increase in current produces a more marked current distribution in all electrodes, evidenced by a higher value of δ_{av}. Likewise, the current distribution at the bipolar electrode is always more uniform than that at the terminal electrodes as a consequence of the damping effect of the resistances of solid and fluid phases. Comparing in Figs. 4 and 5, Part (a) with Part (b) and Part (c) with Part (d) it is observed that more uniform current distributions are obtained when the concentration decreases as a consequence of that the higher solution resistance dampens the current density along the electrode length. Likewise, the increase in concentration, or in conductivity, enlarges the leakage current across the by-pass channel which is mainly supplied by the region near the inlet of electrolyte, increasing the current distribution. Moreover, the comparison in Fig. 4 between Part (a) with Part (c) and Part (b) with Part (d) shows that the diminution of the by-pass resistance increases the leakage current, see Table 4, which favours a more marked current distribution. The effect of the by-pass channel on the current distribution is less significant when the current feeder is placed in the middle point of the terminal electrodes as it is shown by comparison of Part (a) with Part (c) and Part (b) with Part (d) of Fig. 5. In this case it is observed a slight decrease in the mean relative deviation at the terminal electrodes when the size of the by-pass channel is enlarged, which can be explained considering that the increase in leakage current enlarges the current density in the region near the by-pass improving the uniformity of the current distribution. According to Table 4 the confidence intervals, CI, of the cell potential difference and leakage current are narrow given a good reproducibility of the experimental measurements. Likewise, the calculated values of both parameters are very close to the experimental set corroborating the predictive capability of the theoretical model. In Table 4 it must be remarked the important increase of the leakage current for the largest by-pass channel, mainly at the highest value of concentration.

4.4. Comparison of theoretical current distributions in a bipolar electrochemical stack with resistive or equipotential electrodes

Fig. 6 reports on the theoretical current distributions for the bipolar electrochemical reactor with the largest size of the by-pass channel and for the more concentrated electrolyte. These working conditions represent the more critical case for the current distribution. The full and dashed lines correspond to those of Part (d) in Fig. 4 and the dash-dotted lines to the same reactor with nickel electrodes of $\kappa_s = 1.45 \times 10^7\ S\,m^{-1}$, which can be considered as equipotential electrodes for the present conditions of range of

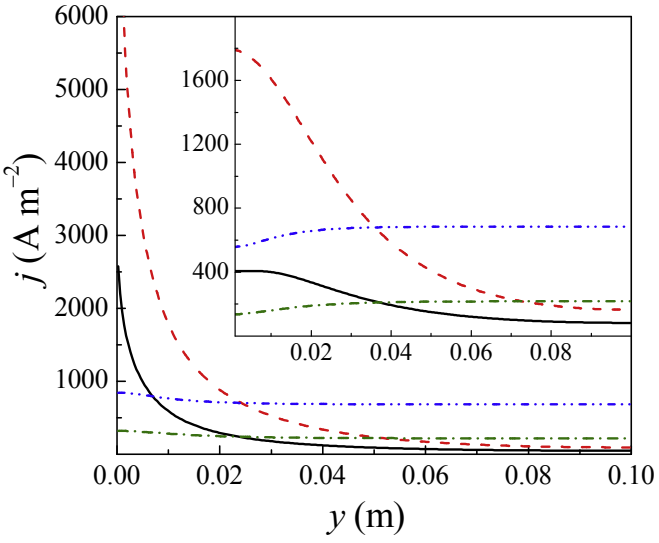

Fig. 6. Comparison of the theoretical current distributions for a bipolar electrochemical stack with resistive or equipotential electrodes. Water electrolysis from alkaline electrolytes. $T \approx 27\,^{\circ}C$. Current feeders placed at the end of the terminal electrodes. By-pass II and [NaOH] = 6 M. Full black lines: numerical calculations for resistive electrodes at $I = 1$ A. Dashed red lines: numerical calculations for resistive electrodes at $I = 3$ A. Dash-dotted green lines: numerical calculations for equipotential electrodes at $I = 1$ A. Dash-double-dotted blue lines: numerical calculations for equipotential electrodes at $I = 3$ A. Insets: current distributions for the bipolar electrode.

Table 5
Comparison between theoretical results of resistive and equipotential electrodes.

	[NaOH] (M)	Electrical connection	I (A)	Difference in U (%)	Difference in I^* (%)
By-pass I	1	Border	1	30.6	19.1
			3	68.1	43.4
		Middle point	1	30.9	−11.5
			3	68.5	−22.4
	6	Border	1	25.0	14.1
			3	58.4	33.4
		Middle point	1	25.4	−9.6
			3	58.9	−17.8
By-pass II	1	Border	1	29.9	19.0
			3	67.0	42.9
		Middle point	1	31.3	−12.7
			3	69.1	−23.2
	6	Border	1	24.0	14.4
			3	57.2	33.1
		Middle point	1	26.0	−12.1
			3	59.5	−19.6

currents and electrode dimensions. Fig. 6 puts on evidence the strong influence of the resistive electrodes on the current distribution affecting negatively the reactor performance. Table 5 shows the percentage differences of cell voltage and leakage current for electrochemical reactors with resistive and activated electrodes, related to the equipotential case. As expected, it can be observed an important increase in the cell potential difference for reactors with resistive electrodes. However, when the current is fed in the middle point of the resistive electrode the leakage current is lower than that of the equipotential case, revealing the great importance of the design of the current feeder.

The results reported on Figs. 4–6 corresponding to sections 4.3 and 4.4 were performed with a structured non-uniform mesh grading of (300,300) cells for the fluid phase and (30,250) cells for each solid phase (anode, cathode and bipolar) in the (x,y) directions. Between 386 and 561 s were required on a 2.5 GHz single core, and 662 to 1463 iterations were needed to reach the final solution with a normalised tolerance of 1×10^{-7} for the potential field in each region. The initial guess values were 0 V for the cathodic region, 10 V for the anodic region, 3 V for the bipolar region and 4 V for the fluid region and applying at the current feeder of the anodic region the boundary condition given by Eq. (7). The above mesh size was chosen after a mesh-independence study similar to the one described in section 4.2.

4.5. Benefits and limitations of the proposed model approach

The main benefits of the proposed tool, considering implications for academic studies and for scale-up and industrial use are: 1) the source code is accessible and modifiable, what means that is suitable for proposing improvements or discovering mistakes; 2) no license costs; 3) wide range of applications and models, already existing in OpenFOAM, ready to couple with the present strategy; 4) the software allows to solve problems under the primary (when kinetic parameters of very fast electrochemical reactions are used) or secondary current distribution hypotheses, assuming that the gas evolving reactions do not influence appreciably the fluid phase; 5) the solver can be applied without restrictions of conductivities of the solid-fluid phases and 6) modifications in the program to take into account the gas phase or a tertiary current distribution can be implemented. As limitation it can be stated that this computational strategy is more technical and it may be harder to use in comparison to commercial software, demanding trained people for its modification.

5. Conclusions

An easy to understand and general strategy was developed, by coupling different regions for the potential field, in order to obtain current density distributions at each electrode, leakage currents and potential cell difference in electrochemical reactors composed of activated or resistive electrodes, under monopolar or bipolar electrical connection. The model allows performing the calculations under galvanostatic control or for a given local potential in any electrode and also for a fixed cell potential difference. Additionally, it accepts as input multiple electrochemical reactions per electrode and extra resistances as a consequence of thin layers over the electrodes or the presence of a gas phase in the electrolyte, given the effective resistivity.

The proposed open source tool, considering secondary current distribution, was validated by comparing with theoretical results from simplified analytical models, with experimental data of previous works and with own experiments, giving in all cases a close agreement between both sets of results with an average value of the mean relative percent error of $8.8 \pm 2.1\%$ for the current distribution taking into account all the experiments. It has been also tested using activated electrodes and kinetic parameters of fast reactions, showing excellent reproducibility of the limit approximations of equipotential electrodes and primary current distribution, respectively. The great effect of the resistive electrodes and the current feeder point on the current distribution is revealed, allowing modifications in order to improve the behaviour of the equipment.

It must be emphasized that the present method can be adapted, by modification of the algorithm, to solve further problems involving concentration or conductivity variations. Thus, the relevant mass-transfer equations in single-phase or two-phase systems must be considered simultaneously with the potential field. The calculation strategy is applicable to conventional electrochemical cell with massive electrodes but also to more complicated electrochemical configurations such as corrosion cells, in which the anodic and cathodic areas are not separated.

Finally, the proposed tool can help the designer in scale-up situations and it allows developing efficient electrochemical reactors by comparing results using different electrode materials, electrolytes and cell designs.

Acknowledgements

This work was supported by Agencia Nacional de Promoción Científica y Tecnológica (ANPCyT), Consejo Nacional de

Investigaciones Científicas y Técnicas (CONICET) and Universidad Nacional del Litoral (UNL) of Argentina.

List of Symbols

A	parameter given by Eq. (11)
A_m	transverse section of the electrolyte manifold, m^2
B	parameter given by Eq. (10)
b	Tafel slope, V
CI	confidence interval, V or mA
E_0	equilibrium potential, V
$e_{s\text{-}f}$	solid electrode thickness or fluid interelectrode gap, m
f	parameter defined in Eq. (12)
G	length of the electrolyte manifold, m
g	functionality given in Eq. (4)
H	electrode height, m
I	current, A
I^*	shunt, leakage or bypass current given by: $I^* = I^T - I^{bip}$, mA
j	current density, A m^{-2}
j_0	exchange current density, A m^{-2}
L	electrode length, m
n	coordinate normal to surface, m
p	p^{th} segmented electrode
r	radial coordinate, m
S	electrode surface area, m^2
T	temperature, °C
U	cell potential difference, V
U_0	reversible cell potential difference, V
VR	function defined in Eq. (12)
VGR	function defined in Eq. (12)
x	axial coordinate, m
y	axial coordinate, m
z	axial coordinate, m

Greek characters

Δ	distance between the cell centre to the interface, m
δ_{av}	mean relative deviation given by Eq. (21)
κ	electrical conductivity, S m^{-1}
ϕ	potential, V
Ω_{av}	mean relative error given by Eq. (22), %

Subscripts

av	average
bp	boundary patch
CF	current feeder
exp	experimental
f	fluid phase
k	anodic or cathodic interface
s	solid phase
the	theoretical
w	wall
y	variable referred to the y coordinate

Superscript

bip	bipolar electrode
i	i^{th} reaction
p	p^{th} segmented electrode
T	terminal electrode

References

[1] J. Newman, K.E. Thomas-Alyea, Electrochemical Systems, third ed., Wiley-Interscience, 2004.
[2] A.C. West, Electrochemistry and Electrochemical Engineering: an Introduction, CreateSpace Independent Publishing Platform, 2012.
[3] A.N. Colli, J.M. Bisang, Validation of theory with experiments for local mass transfer at parallel plate electrodes under laminar flow conditions, J. Electrochem. Soc. 160 (2013) E5.
[4] A.N. Colli, J.M. Bisang, Mass-transfer characterization in a parallel-plate electrochemical reactor with convergent flow, Electrochim. Acta 113 (2013) 575.
[5] A.N. Colli, J.M. Bisang, The effect of a perpendicular and cumulative inlet flow on the mass-transfer distribution in parallel-plate electrochemical reactors, Electrochim. Acta 137 (2014) 758.
[6] A.N. Colli, J.M. Bisang, Combination of cumulative and convergent flows as a means to improve the uniformity of tertiary current distribution in parallel-plate electrochemical reactors, J. Electrochem. Soc. 164 (2017) E42.
[7] L.F. Arenas, C. Ponce de León, F.C. Walsh, Engineering aspects of the design, construction and performance of modular redox flow batteries for energy storage, J. Energy Storage 11 (2017) 119.
[8] A.N. Colli, P. Peljo, H.H. Girault, High energy density MnO_4^-/MnO_4^{2-} redox couple for alkaline redox flow batteries, Chem. Commun. 52 (2016) 14039.
[9] M. Matlosz, P.H. Vallotton, A.C. West, D. Landolt, Nonuniform current distribution and thickness during electrodeposition onto resistive substrates, J. Electrochem. Soc. 139 (1992) 752.
[10] W.H. Smyrl, J. Newman, Current distribution at electrode edges at high current densities, J. Electrochem. Soc. 136 (1989) 132.
[11] T.-C. Chang, J.-P. Zhang, Y.-K. Fuh, Electrical, mechanical and morphological properties of compressed carbon felt electrodes in vanadium redox flow battery, J. Power Sources 245 (2014) 66.
[12] L.D. Brown, T.P. Neville, R. Jervis, T.J. Mason, P.R. Shearing, D.J.L. Brett, The effect of felt compression on the performance and pressure drop of all-vanadium redox flow batteries, J. Energy Storage 8 (2016) 91.
[13] J. Wojtowicz, L. Laliberté, B.E. Conway, Current distribution and potential profile at a linear wire electrode of significant ohmic resistance, Electrochim. Acta 13 (1968) 361.
[14] J.M. Bisang, G. Kreysa, Study of the effect of electrode resistance on current density distribution in cylindrical electrochemical reactors, J. Appl. Electrochem. 18 (1988) 422.
[15] J.M. Bisang, The effect of metal and solution phase resistances on the current distribution in cylindrical electrochemical reactors, J. Appl. Electrochem. 19 (1989) 500.
[16] F.H. Edelman, R.W. Klopfenstein, Shaped electrode design, J. Electrochem. Soc. 112 (1965) 109.
[17] N. Ipek, A. Cornell, M. Vynnycky, A mathematical model for the electrochemical pickling of steel, J. Electrochem. Soc. 154 (2007) P108.
[18] K. Wu, E. Birgersson, B. Kim, P.J.A. Kenis, I.A. Karimi, Modeling and experimental validation of electrochemical reduction of CO_2 to CO in a microfluidic cell, J. Electrochem. Soc. 162 (2015) F23.
[19] I. Rousar, J. Thonstad, Calculation of bypass currents in molten salt bipolar cells, J. Appl. Electrochem. 24 (1994) 1124.
[20] A.N. Colli, H.H. Girault, Compact and general strategy for solving current and potential distribution in electrochemical cells composed of massive monopolar and bipolar electrodes, J. Electrochem. Soc. 164 (2017) E3465.
[21] E.R. Henquín, J.M. Bisang, Effect of leakage currents on the secondary current distribution in bipolar electrochemical reactors, J. Appl. Electrochem. 38 (2008) 1259.
[22] G.A. Prentice, C.W. Tobias, Finite difference calculation of current distributions at polarized electrodes, AIChE J. 28 (1982) 486.
[23] H.G. Weller, G. Tabor, H. Jasak, C. Fureby, A tensorial approach to computational continuum mechanics using object-oriented techniques,, Comput. Phys. 12 (1998) 620.
[24] G. Kreysa, H.J. Külps, Experimental study of the gas bubble effects on the IR drop at inclined electrodes, J. Electrochem. Soc. 128 (1981) 979.
[25] D. Bergner, K. Hannesen, Operating experience gained with the bipolar Hoechst-Uhde membrane cell, in: K. Wall (Ed.), Modern Chlor-alkali Technology, Ellis Horwood Ltd., Chichester, 1986, p. 162.
[26] N. Guillet, P. Millet, Alkaline water electrolysis, in: G.-J. Agata (Ed.), Hydrogen Production by Electrolysis, Wiley-VCH Verlag GmbH & Co. KGaA, 2015, p. 117.
[27] J. Newman, Engineering design of electrochemical systems, Ind. Eng. Chem. 60 (1968) 12.
[28] H.K. Versteeg, W. Malalasekera, An Introduction to Computational Fluid Dynamics: the Finite Volume Method, Pearson Education Limited, 2007.
[29] F. Moukalled, L. Mangani, M. Darwish, The Finite Volume Method in Computational Fluid Dynamics: an Advanced Introduction with OpenFOAM® and Matlab®, Springer International Publishing, 2015.
[30] T.M. Braun, D.T. Schwartz, Localized electrodeposition and patterning using bipolar electrochemistry, J. Electrochem. Soc. 162 (2015) D180.
[31] A.N. Colli, https://github.com/ancolli/secondaryCurrentDistributionFoam, 2018.
[32] https://openfoam.org.
[33] P. Qian, H. Zhang, J. Chen, Y. Wen, Q. Luo, Z. Liu, D. You, B. Yi, A novel electrode-bipolar plate assembly for vanadium redox flow battery applications, J. Power Sources 175 (2008) 613.
[34] R.M. Darling, H.-S. Shiau, A.Z. Weber, M.L. Perry, The relationship between shunt currents and edge corrosion in flow batteries, J. Electrochem. Soc. 164 (2017) E3081.
[35] J.M. Bisang, Simultaneous solution of the potential equations for the metal and solution phases in cylindrical electrochemical reactors, J. Appl. Electrochem. 20 (1990) 723.